

Three-dimensional refined analysis of seismic cracking and anti-seismic measures performance of concrete face slab in CFRDs

Yongqian Qu, Degao Zou^{*}, Kai Chen, Jingmao Liu

State Key Laboratory of Coastal and Offshore Engineering, Dalian University of Technology, Dalian 116024, China
School of Hydraulic Engineering, Dalian University of Technology, Dalian 116024, China

ARTICLE INFO

Keywords:

Concrete faced rockfill dam
Concrete face slab
Seismic cracking
Anti-seismic measures
Elasto-plastic analysis

ABSTRACT

The concrete face slab is the primary anti-seepage component of concrete faced rockfill dams (CFRDs). Therefore, the seismic safety of the slab is an important issue. In this paper, the cohesive zone model and the explicit solution are expanded to conduct 3D seismic failure analysis of a CFRD. A combination of the generalized plasticity model of rockfill, state-dependent elasto-plastic model of soil-structure interfaces, a non-uniform wave input method and the scaled boundary finite element method is used to perform an elasto-plastic, cross-scale analysis of the seismic cracking evolution of concrete face slabs. The above combined method is used to investigate the cracking mechanism, cracking characteristics and potential anti-seismic measures. The results indicate that the cyclic deformation caused by the earthquake results in the formation of horizontal, connected cracks in the middle of the slab at 70–75% of the dam height. In addition, the plastic deformation of the rockfill leads to the formation of horizontal, unconnected cracks on both sides of the slab at 85% of the dam height. A comprehensive anti-seismic measure is proposed based on material property improvement and structural optimization, decreasing the maximum crack width and the total crack length by 21% and 89.9%, respectively.

1. Introduction

Concrete faced rockfill dams (CFRDs) have become a more popularly implemented dam type due to reliability, cost effectiveness and the adaptability to various environments and climates (Kim and Kim, 2008; Kartal et al., 2010; Zarfl et al., 2015). Many high CFRDs are constructed in meizoseismal areas, such as the Jinglintai dam (height of 157 m), the Zipingpu dam (height of 156 m), and the Gongboxia dam (height of 132 m) (Qu et al., 2019). Therefore, the seismic safety of these dams has received widespread concern and attention. The concrete face slab is the primary anti-seepage structure in the CFRD and can be destroyed during an earthquake, i.e., the cracking of the Cogawell CFRD in Whittier Narrows earthquake (1991) (Boulanger et al., 1995) and dislocation and extruding damage of Zipingpu CFRD in the Wenchuan earthquake (2008) (Kong et al., 2011; Zou et al., 2012). The safety and integrity of the face slab plays a key role in the seismic safety of the CFRDs (Kong et al., 2016; Arici, 2013). Therefore, it is necessary to study the seismic failure characteristics and anti-seismic measures of face slabs.

CFRD is a three-dimensional, nonlinear and discontinuous complex system (Fig. 1). However, dynamic analyses of CFRDs are at present commonly simplified using linear or equivalent linear methods (Kong

et al., 2016). However, this method cannot describe the evolution of plastic deformation, which is one of the most important properties of rockfill and an important cause of slab damage. Meanwhile, the current linear elastic models for the face slab cannot describe stiffness degradation and strain softening of concrete, which happens during the failure process. As a result, the linear elastic models often yield large-scale, excessive stresses that exceed the tensile strength of concrete. Concrete is a quasi-brittle material, and thus as the tension increases, the concrete starts to crack and experience stiffness degeneration and strain softening, which is often accompanied by local narrow-band fracturing. Linear elastic models consequently are unsuitable for the study of damage evolution and for evaluating the anti-seismic performance of concrete face slabs. Therefore, an adequate seismic analysis of CFRDs requires a shift from the use of equivalent linear analysis to methods that can accommodate strongly nonlinear and elasto-plastic events.

The rapid development of computational power in the recent years have enabled more researchers to conduct nonlinear and elasto-plastic analyses of the CFRD. The elasto-plastic models for rockfill and the interface between soil and structure have been studied extensively and applied to the simulation of CFRDs. Results from the studies provide the foundation for developing ways to perform failure analysis of face slabs.

^{*} Corresponding author at: State Key Laboratory of Coastal and Offshore Engineering, Dalian University of Technology, Dalian 116024, China.
E-mail address: zoudegao@dlut.edu.cn (D. Zou).

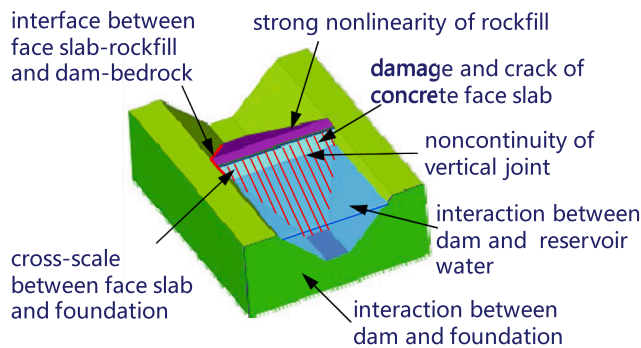


Fig. 1. Difficulties in seismic failure simulation of concrete face slabs.

Despite the availability of analytic methods to address the treatment of crack in media (Ahmadi and Eskandari, 2013, 2014; Ahmadi et al., 2016; Li et al., 2020; Yang et al., 2020), the scale of CFRD is too large and difficult to solve. Therefore, numerical simulation is the primary method for investigating the failure characteristics of face slab. Recent research efforts include the introduction of nonlinear models of concrete for the analysis of CFRDs. Such models include the plastic damage model, the fixed crack model, the damage model, etc. (Qu et al., 2019; Xu et al., 2015; Arici, 2011). However, most of these models are applied to two-dimensional analysis, and while the models can provide a qualitative description of the dynamic damage characteristics of the dam, they are unable to consider three-dimensional effects. Therefore, it is difficult to evaluate the seismic performance of CFRD reasonably and accurately. Researchers such as Dakoulas (2012) and Cen et al. (2016) carried out 3D analyses with nonlinear models of the concrete face slab, but the overall framework of their simulations rely on equivalent linear methods. In other words, there is a lack of efforts dedicated to the 3D, nonlinear and elasto-plastic analysis of whole CFRDs with particular emphasis on the seismic failure characteristics of the face slab.

The difficulty of the whole, elasto-plastic seismic failure analysis of 3D CFRD lies in model construction, efficiency and convergence. CFRDs are large scale projects and are cross-scale structures. The dimensions of key structures often differ by magnitudes of order. For example, the thickness of the slab is measured in decimeters but the length of the rockfill area and foundation is several hundred meters. Research has shown that fine meshes are necessary for simulating damaged areas (Qu et al., 2017), thus requiring the face slab to be modeled with highly refined meshes in order to allow for proper failure analysis. However, extending the refined mesh uniformly to the rockfill area and foundation will generate tens of millions of elements (Chen et al., 2018a), resulting in an impractical computational burden, especially in the context of 3D elasto-plastic seismic analysis. In addition, the elasto-plastic constitutive models of rockfill, interface and concrete are complex and time-consuming to solve; thus the dynamic response of the CFRD is most often analyzed implicitly. However, implicit solver has difficulty in convergence when the CFRD is excited by an intense earthquake, which can bring about strongly nonlinear, large deformations and discontinuous characteristics that are present in events such as slipping of the dam slope, separation between slab and cushion, cracking of the slab, opening of joints etc. Such events make convergence difficult and can even degrade the accuracy of implicit methods. The explicit solver avoids nonlinear iteration, the problem of divergence, and the need to solve equation groups.

Cross-scale analysis is an alternative approach to solve the above problems and is gradually being introduced to simulate CFRDs. Zhou et al. (2016, 2018) demonstrated the feasibility of implementing coarse-fine mesh transitions through the application of nonlinear contact mechanics and the substructure method. They studied the axial compression, the slab-slab separation and the face-rockfill separation of Tianshengqiao-I CFRD under static loads. Using the framework of the dual mortar finite element method, Wang et al. (2019) presented a

numerical approach by considering the contact bodies as independent porous media continuums. Then, the method was used to investigate the discontinuous separation and sliding between concrete gallery of the Rumei clay-core rockfill dam. Chen et al. (2017, 2018a, 2018b, 2019) modified the polygon scale boundary finite element method (SBFEM) to perform cross-scale analysis of CFRDs. Qu et al. (2017, 2018) and Gong et al. (2019) conducted cross-scale analysis of soil-structure interaction through using the asymmetric interface element and the meshless method. These studies provide the basis for 3D cross-scale analysis of CFRD.

In this paper, the concrete cohesive zone model (CZM) and the explicit method are expanded to perform a 3D seismic failure analysis of CFRDs. The 3D elasto-plastic seismic cracking evolution of the concrete face slab in the CFRD is simulated through the following components: a generalized plastic model of rockfill, a state-dependent elasto-plastic model of the interface and a non-uniform wave input method. The cross-scale model of a 150 m high 3D CFRD is established and analyzed by SBFEM-FEM to finely and efficiently investigate the failure mechanisms and characteristics of the face slab. Finally, a comprehensive anti-seismic measure for the face slab is proposed from the perspective of material improvement and structural optimization. The proposed method can directly reproduce the dynamic cracking evolution process of the face slab, accurately locate the local vulnerable areas, and quantify the damage severity and provide insight into the effect of anti-seismic measures. The results can provide guidance for the anti-seismic optimal design of concrete face slabs and the evaluation of the ultimate anti-seismic capacity of CFRDs.

2. Theoretical method

2.1. Cohesive zone model

The cohesive zone model (CZM) is one of the most used approaches to describe the fracture behavior of concrete. The concept of CZM was first proposed by Barenblatt (1962) and Dugdale (1960) and was further extended to the concrete cracking simulation by Hillerborg et al. (1976). CZM is rooted in elasto-plastic mechanics and describes the separation of an interface by the resistance of cohesive forces. Stress is treated as a function of displacement during cracking, thus avoiding the singularity issue that has been encountered in linear elastic fracture mechanics (Dai and Ng, 2014). This model has been widely applied to simulate tensile fractures in concrete (Yilmaz and Molinari, 2017; Trawiński et al., 2018; Kim et al., 2015) and have been implemented for several concrete dam (Zhong et al., 2018; Pan et al., 2011). However, there are limited research efforts and reported applications of CZM in the modeling of CFRDs.

The authors have applied CZM to the two-dimensional simulation of CFRDs and have proven the feasibility of CZM in the seismic failure analysis of concrete face slabs (Qu et al., 2020). However, the 2D analysis cannot describe the 3D characteristics of the CFRD (e.g. vertical joints, valley shape, axial ground motion, etc.), therefore, it is difficult to accurately and reasonably evaluate the seismic safety of face slab. Meanwhile, challenges relating to the modeling, computational burden, efficiency, convergence and other problems in 3D simulation become exacerbated. This paper first develops the 3D seismic cracking method of face slab using methods developed in previous work. Then, the seismic failure mechanism and failure properties of concrete face slab are investigated. Finally, the anti-seismic measures for face slab are proposed and evaluated.

When the CZM is used to simulate cracking, the cohesive interface element (CIE) should be embedded in the area of potential failure. The CIEs are connected to the surrounding solid elements, as shown in Fig. 2. During the loading process, the stresses of the CIE reaches the cracking criterion, upon which the stiffness and bearing capacity of the CIE decreases gradually. When the stiffness decreases to zero, the CIE fails and a new crack appears. The bilinear CZM is suitable for describing the

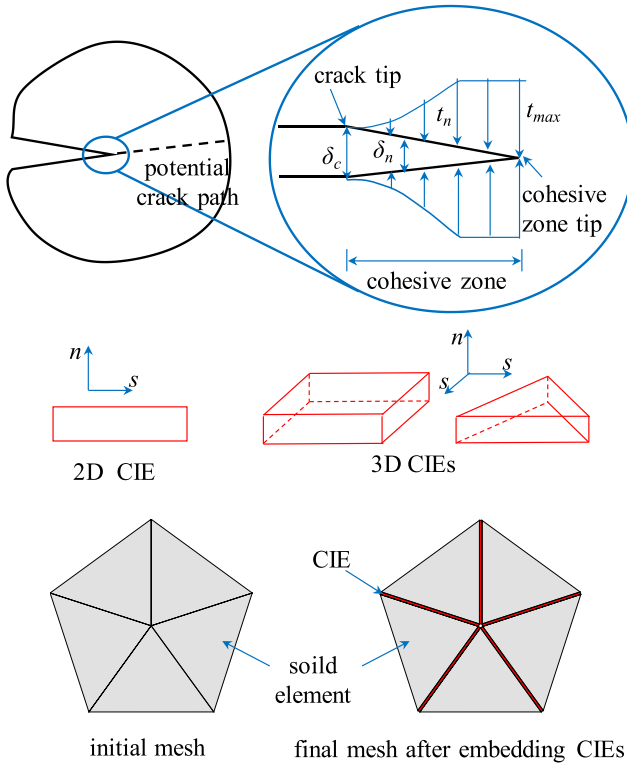


Fig. 2. Cohesive zone model and cohesive interface elements.

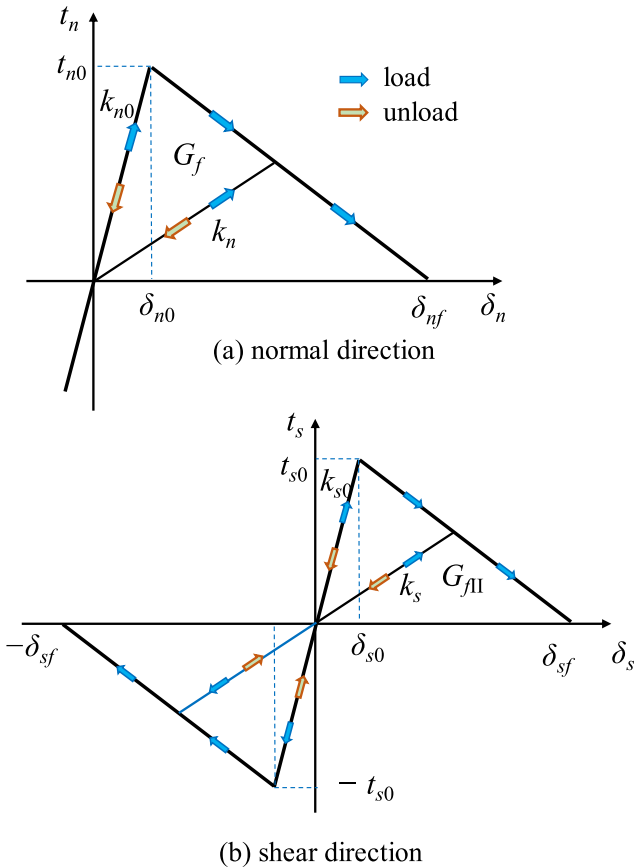


Fig. 3. Relationship between traction and displacement.

fracture of brittle materials and has a high computational efficiency (Alfano, 2006). Therefore, the bilinear CZM is adopted to describe the failure characteristics of concrete face slab, as shown in Fig. 3.

The initial damage of the element is determined by the criterion of square nominal stress:

$$\left(\frac{\langle t_n \rangle}{t_{n0}}\right)^2 + \left(\frac{t_s}{t_{s0}}\right)^2 + \left(\frac{t_t}{t_{t0}}\right)^2 = 1 \quad (1)$$

where t_n , t_s and t_t are normal and shear stresses respectively; t_{n0} , t_{s0} and t_{t0} are maximum allowable stresses at normal and shear direction respectively. McCauley brackets are used to distinguish between compression and tension.

$$\langle t_n \rangle = \begin{cases} t_n, & t_n \geq 0 \\ 0, & t_n < 0 \end{cases} \quad (2)$$

The damage factor is used to describe the degradation of interface stiffness after damage has occurred. Without considering the interaction between normal and tangential directions, the relationship between stress and displacement is

$$\mathbf{t} = \begin{Bmatrix} t_n \\ t_s \\ t_t \end{Bmatrix} = (1 - d)\mathbf{K} \begin{Bmatrix} \delta_n \\ \delta_s \\ \delta_t \end{Bmatrix} + d\mathbf{K} \begin{Bmatrix} \langle -\delta_n \rangle \\ 0 \\ 0 \end{Bmatrix} \quad (3)$$

$$\mathbf{K} = \text{diag}(k_{n0} \quad k_{s0} \quad k_{t0}) \quad (4)$$

where δ_n , δ_s and δ_t are the normal and shear displacements respectively, k_{n0} , k_{s0} and k_{t0} are the normal and shear elastic modulus respectively, d is the damage factor and is a function of the effective displacement δ_m

$$d = \frac{\delta_f(\delta_{max} - \delta_0)}{\delta_{max}(\delta_f - \delta_0)} \quad (5)$$

$$\delta_m = \sqrt{\langle \delta_n \rangle^2 + \delta_s^2 + \delta_t^2} \quad (6)$$

where δ_0 is the initial cracking displacement, δ_{max} is the maximum effective displacement in the loading history, and δ_f is the displacement at the failure stage.

The fracture energy is the area within the curve shown in Fig. 3 and can be expressed as

$$G = \int_0^{\delta_f} t(\delta) d\delta = \frac{1}{2} t_0 \delta_f \quad (7)$$

where t_0 is the cohesive strength.

2.2. Generalized plastic model of rockfill

The generalized plastic model (Pastor et al., 1985; Pastor and Zienkiewicz, 1986) was first proposed by Pastor and Zienkiewicz mainly for describing the liquefaction of sand under low confining pressure (Pastor and Zienkiewicz, 1986). The deformation of the rockfill is pressure dependent and the confining pressure in a high dam is very high, which limits the application of generalized plastic model in the static and dynamic analyses of high earth rock dams. Based on the generalized plastic model of sand, a model was developed (Xu et al., 2012; Zou et al., 2013) to take into account the pressure dependence and cyclic hysteretic properties of the rockfill. The model was applied to the dynamic elastoplastic analysis of a earth rock dam and recreate the seismic deformation of the Zipingpu CFRD as caused by the Wenchuan Earthquake (Xu et al., 2015; Qu et al., 2017; Xu et al., 2012; Zou et al., 2013). Further details about the formulations and parameters can be found in the literature (Xu et al., 2012; Zou et al., 2013).

2.3. The elasto-plastic model of the soil-structure interface

The mechanical properties of the interface between soil and structure have an important influence on the stress and deformation of the structure. Contact problems between soil and structure in practical engineering are three-dimensional (Zhang et al., 2008). However, most of the current interface constitutive models assume that the two shear directions are independent of each other, which is inaccurate according to three-dimensional contact tests (Evgin and Fakharian, 1996). To solve this problem, a three-dimensional elasto-plastic model of interface was proposed by Liu et al. (2014), and has been applied to simulate the interaction between the face slab and the cushion during different scenarios, including construction, water storage and seismic excitation (Liu et al., 2015). The main characteristics of the model are as follows: 1) the monotonic and cyclic deformation characteristics of the interface with different void ratios and normal boundary conditions can be described without changing parameters. 2) The coupling between two perpendicular shear deformations (i.e. the three-dimensional effect of interface deformation) can be considered. 3) The influence of particle breakage under monotonic and cyclic loading and the phenomenon of large normal displacements under cyclic loading can be considered. Additional details about the derivations and the parameters can be found in (Liu et al., 2014).

2.4. Non-uniform seismic wave input method

The dam-valley-foundation is an open energy system (Xu et al., 2018). There are different degrees of interaction between the valley, foundation and dam. Meanwhile, the external scattered energy will radiate to the infinite foundation. These will lead to the difference in the dynamic response at each point of the dam boundary.

In addition, with the increase in dam height, and with the dam axial/horizontal length exceeding 1000 m, the effect of seismic wave characteristics on the seismic response of the CFRD can be significant. Therefore, the non-uniform seismic wave input method is necessary to investigate the seismic response of the CFRD. The non-uniform seismic wave input method is realized using a viscous-spring artificial boundary and equivalent nodal loads (Liu et al., 2006).

For the three-dimensional viscous-spring artificial boundary, the element spring coefficients, K , and damping coefficients, C , are

$$K = \alpha \frac{G}{r} \sum_{i=1}^I A_i \quad (8)$$

$$C = \rho c \sum_{i=1}^I A_i \quad (9)$$

where G is shear stiffness of the material at the boundary, ρ is density, r is the distance from the scattering source to the artificial boundary node, c is wave velocity, α is the parameter of the boundary in different directions, A_i is the area represented by the boundary node.

The expression of equivalent nodal load is

$$F_b = R_b^{ef} + C_b v_b^{ef} + K_b u_b^{ef} \quad (10)$$

where u_b^{ef} , v_b^{ef} and R_b^{ef} are respectively the displacement vector, velocity vector and the corresponding force vector induced at the system boundary nodes by the free wave field, and K_b and C_b are respectively the additional stiffness matrix and damping matrix of the boundary elements.

2.5. Scaled boundary finite element method (SBFEM)

The scaled boundary finite element method (SBFEM) was proposed in 1997 (Wolf and Song, 1996; Wolf and Schanz, 2004). It is a semi analytical method and inherits the advantages of the boundary element

method. SBFEM can deal with polyhedral elements with an arbitrary number of sides and has inherent advantages in the generation of cross-scale meshes. Due to the radial analytical solution, the method cannot describe the internal yielding stress of the element and solve nonlinear problems, which limits the application of SBFEM towards elasticity analyses (Man et al., 2012; Liu et al., 2016; Liu and Gao, 2012; Shi et al., 2013). However, material nonlinearity is often an unavoidable technical problem when conducting numerical analyses, especially in geotechnical engineering. Chen et al. (2017, 2018b, 2019) is the first to reconstruct the element interpolation function and displacement strain matrix for nonlinear analysis through the original boundary Gauss integral point of SBFEM. The correlation coefficient matrices were computed using the constant stiffness matrix of materials. Secondly, by adding Gauss points in the elements, the displacement strain coordination matrix, stiffness matrix and stress integration were computed by an internal integration scheme. Finally, the nonlinear polyhedral SBFEM was established and demonstrated for the elasto-plastic analysis of CFRDs. The modified SBBEM has shown a good prospect for practical use in geotechnical engineering (Chen et al., 2021; Zou et al., 2019).

2.6. Central difference method

The central difference method is the most used explicit method in FEM. The node acceleration at time t is

$$\ddot{u}_i = M^{-1}(P - I)_i \quad (11)$$

The quality matrix used in the explicit solver is diagonal matrix, which avoids the simultaneous solving of multiple equations, thus making the solving process very efficient and resource saving. If the acceleration is constant in a very short time, the center difference algorithm can be used to integrate the acceleration and calculate the node velocity

$$\dot{u}_{t+\Delta t/2} = \dot{u}_{t-\Delta t/2} + \frac{\Delta t + \Delta t}{2} \ddot{u}_i \quad (12)$$

Then, the node displacement is calculated by the velocity integral of the center difference

$$u_{t+\Delta t} = u_t + \Delta t + \Delta t \dot{u}_{t+\Delta t/2} \quad (13)$$

where Δt is the time step. The central difference method is conditionally stable. It will be numerically unstable when the time step is greater than the maximum allowable value. The critical time step of central difference method is

$$\Delta t_{crit} = \min_i \frac{2}{\omega_i} (\sqrt{\xi_i^2 + 1} - \xi_i) \quad (14)$$

where ω_i is the i^{th} frequency, ξ_i is the damping ratio of the system at the i^{th} frequency.

3. Model of 3D concrete faced rockfill dam

3.1. Cross-scale FEM-SBFEM model

The 150 m high 3D CFRD is used to investigate the seismic failure characteristics of the face slab, as shown in Fig. 4. The upstream slope and downstream slope have ratios of 1:1.4 and 1:1.6, respectively, and the bank slopes on both sides have a ratio of 1.0:1.0. The dam crest width is 16 m, and the valley width is 50 m. The depth of the bedrock is 100 m, and the width of the side bedrock is 150 m. The thicknesses of the face slab at the crest and the bottom are 0.3 m and 0.87 m, respectively. Both the vertical and axial mesh sizes of the face slab are 1.0 m. The face slab is simulated by eight-node isoparametric elements and CIEs are embedded among all the elements, as shown in Fig. 4(b). The double-layer steel mesh is set in the slab and simulated by bar elements. A cross-scale model is established and analyzed by using SBFEM-FEM, as

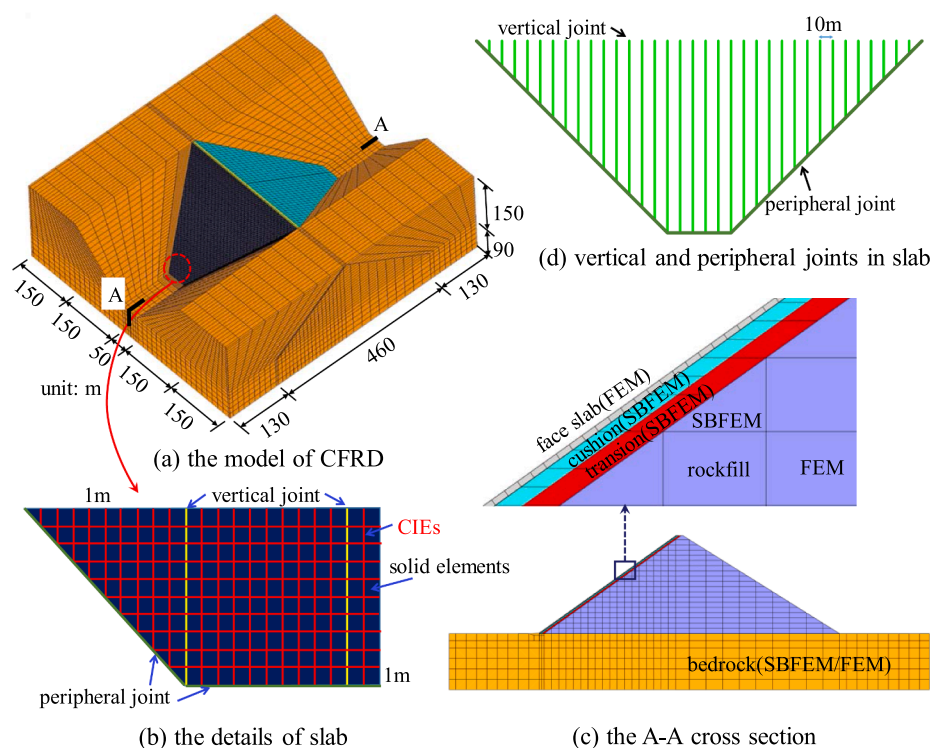


Fig. 4. Cross-scale model of 3D CFRD.

shown in Fig. 4(c). Interface elements are set between the face slab and cushion and between the rockfill and bedrock. Peripheral joints are set between the face slab and the bedrock. Vertical joints are set at the face slab at intervals of 10 m, as shown in Fig. 4(d). The detailed description of mesh sizes, methods, element types and related constitutive models of the model is summarized in Table 1.

In the simulation, the dam is filled in 20 steps and impounded to 144 m in 72 steps. The static simulation includes effects from gravity and water pressure. A seismic excitation is applied under the static state and the interaction between dam and reservoir water is simulated by the added mass method (Westergaard, 1933).

Table 1
The details of the model.

Zone/part	Mesh size	Method	Element type	Constitutive model
face slab	1.0 m	FEM	8-node isoparametric element	Elastic model
vertical joint (slab-slab)	0.02 m (thickness)	FEM	CIE	CZM
	0.02 m (thickness)	FEM	Goodman element	Elastic model
peripheral joints (slab-bedrock)	0.02 m (thickness)	FEM	Goodman element	Elastic model
Interface (slab-cushion)	0.02 m (thickness)	FEM	Goodman element	Elasto-plastic model
Cushion	2.0 m	SBFEM	polyhedron	Generalized plastic model
transition	4.0 m	SBFEM	polyhedron	Generalized plastic model
rockfill	8.0 m	SBFEM/ FEM	polyhedron/8-node isoparametric element	Generalized plastic model
bedrock	2.0–16.0 m	SBFEM/ FEM	polyhedron/8-node isoparametric element	Elastic model

3.2. Material parameters

The parameters of the generalized plastic model for the rockfill and cushion based on large-scale triaxial tests of a CFRD built in China are listed in [Table 2](#). The material parameters ([Qu et al., 2017](#)) of the interface between the face slab and the cushion layer are listed in [Table 3](#). The parameters ([Xu et al., 2015](#)) of the CZM are listed in [Table 4](#) to simulate the CIEs embedded in face slab, and the initial modulus is equal to the concrete ($E = k_n \times d$, $G = k_s \times d$, where E and G are the elastic and shear modulus, respectively, and d is the thickness of CIE). A linear elastic model is used for describing the bedrock and the solid elements of face slab, and its parameters are listed in [Table 5](#). The bidirectional reinforcement ratio is 1.2%. The rebar is simulated using an ideal elasto-plastic model with elastic modulus $E = 200\text{GPa}$ and yield strength $f_v = 400\text{ MPa}$ ([Qu et al., 2019](#)).

The parameters for the joints are as recommended by Zou et al. (Zou et al., 2009). The compressive stiffness of the joints is 25 GPa/m, which is equivalent to wood. The tensile stiffness is 5 MPa/m, and the shear stiffness is 1 MPa/m.

3.3. Input ground motion

The non-uniform seismic wave input method as introduced in above is applied to describe the interaction between the dam and the foundation. The input ground motion is a simulated seismic wave based on the response spectrum obtained from the earthquake risk analysis of a CFRD built in China. The peak ground accelerations (PGA) in the horizontal direction (along the river) and axial direction (perpendicular to the river) are 0.3 g, and the vertical PGA is 0.2 g. The acceleration time history and response spectrum of the seismic wave are shown in Fig. 5. The selected duration of seismic wave is 20.00 s

Table 2

Generalized plastic model parameters of rockfill and cushion.

zone	G_0	K_0	M_g	M_f	α_f	α_g	H_0	H_{U0}	m_s
rockfill	1021	1362	1.7	1.53	0.11	0.11	650	1300	0.44
cushion	965	1288	1.68	1.3	0.10	-0.4	550	1100	0.23
zone	m_v	m_l	m_u	r_d	γ_{DM}	γ_u	β_0	β_1	
rockfill	0.44	0.5	0.5	110	50	5	30	0.025	
cushion	0.23	0.45	0.45	110	50	5	20	0.02	

Table 3

Generalized plastic interface model parameters.

D_{s0} (kPa)	D_{n0} (kPa)	M_c	e_r	λ	$a/kPa^{0.5}$	b	c
1000	1500	0.88	0.4	0.091	224	0.06	3.0
a	r_d	k_m	M_f	k	H_0 (kPa)	f_b	t/m
0.65	0.2	0.6	0.65	0.5	8500	2	0.1

Table 4

The normalized parameters of the cohesive zone model.

k_n (GPa/m)	k_s (GPa/m)	C (MPa)	G (N·m ⁻¹)	d (m)
1550	662.5	3.48	325	0.02

Table 5

Parameters of slab and bedrock.

zone	E (GPa)	ρ (kg/m ³)	ν
slab	31	2500	0.17
bedrock	10	2400	0.25

4. Seismic failure analyses of the concrete face slab

4.1. Failure characteristics

4.1.1. Elastic analysis of face slab

The seismic analysis of the concrete face slab starts with an elastic analysis of the concrete face slab without CIEs. Fig. 6 shows the envelope of the maximum tensile stress (including effects from loads present at static conditions) of the face slab during the earthquake. The excessive tensile stresses (greater than 3.48 MPa) of the face slab are located about 0.5–0.9H (H is the dam height) in the middle of the valley, and about 0.9H in both sides. The angles between stress vectors that exceed the tensile strength and the slope direction of the slab are shown in Fig. 7. The figure shows that the vectors and the slope direction are mostly in alignment, with angular differences below 3°. Therefore, tensile cracks may propagate along the dam axial direction.

The maximum tensile stress exceeds 7.30 MPa, which is far greater than the tensile strength of concrete; furthermore the area experiencing excessive tensile stresses is very large. Similar results can be found in references (Feng et al., 2010; Zhang et al., 2017). These features do not reflect the failure characteristics of concrete. Therefore, the elastic analysis is insufficient for evaluating the seismic performance of the face slab.

4.1.2. Failure analysis of face slab

Starting from this section, the model with CIEs is used to investigate the failure characteristic of the concrete face slab. Fig. 8 shows the positions of damages and the maximum crack width of the face slab during the earthquake. The location of the fracture overlaps with the area prone to excessive tensile stresses (as shown in Fig. 6) as predicted by the elastic model. Xu et al. (2015) conducted 2D dynamic damage analysis of the face slab in a CFRD, and the damage zone (0.65–0.85H) is consistent with this paper. In this model, the CZM describes the stiffness

degradation and softening characteristics of concrete after cracking. Thus, the failure mode is localized and narrow, which is consistent with the damage characteristics of concrete. Meanwhile, excessive tensile stresses occur along the slope (as shown in Fig. 7), and therefore the cracks propagate horizontally.

The maximum cracks during earthquake are summarized in Table 6. There are three connected horizontal cracks at 0.7H, 0.72H and 0.75H in the middle of the valley. The most severe damage occurs at 0.75H, and the crack extends between 110 and 220 m in the axial direction with a total length of 110 m and has a maximum crack width of 9.6 mm. At 0.72H, the crack spans between 140 and 160 m in the axial direction and has a width of 2–7 mm. Finally, at 0.7H, the crack crosses 160–180 m in the axial direction and has a width of 2–5 mm. There are unconnected horizontal cracks at 0.85H on both sides of the slab. The cracks on the left side are distributed between 30 and 110 m along the axial direction. The cracks have a cumulative length of about 39 m and a width of less than 5 mm. Meanwhile, the cracks on the right side are located between 300 and 312 m along the axial direction. The cumulative length of the cracks is about 6 m and a width of no more than 3 mm.

Fig. 9 shows the distribution of cracks after the earthquake and Table 7 summarizes the length and width of residual cracks. Due to the residual deformation of the rockfill, residual cracks are present in the face slab. Compared to the crack distribution shown in Fig. 8, the number of cracks wider than 0.2 mm is reduced, and the lengths of the residual cracks are 30 m, 135 m and 4 m at left, middle and right sections of the slab, respectively. The widest residual crack (2.8 mm wide) is located at 0.75H in the middle of the valley. The crack widths on both sides of the slab range between 1 and 3 mm. Although the earthquake generated higher maximum crack widths (Fig. 8), the cracks rapidly returned to thinner widths. On the other hand, the information about residual cracks has more practical usage, and provides a foundation for further analysis and safety evaluation (such as seepage, etc.). Therefore, residual crack width should be used to evaluate the seismic safety of face slab.

The developed method can describe the stiffness degradation and softening characteristics of post-failure concrete. The computed failure mode of the slab agrees well with the material characteristics of concrete. Meanwhile, the method can describe the evolution of cracks during the earthquake and can directly predict the crack width, thereby allowing the quantitative evaluation of the severity of failure. The method therefore overcomes the limitations of traditional evaluation methods that are based solely on strength standards in linear elastic analysis.

4.2. Failure mechanism

The simulated cracks are connected in the middle and unconnected on both sides of the slab. The difference of failure mode is caused by differences in the mode of deformation.

4.2.1. Side banks of the slab: unconnected cracks

The left bank of the slab is selected as an example for analysis. The deformation and tensile stresses greater than 1.5 MPa before cracking are shown in Fig. 10(a). The deformation and cracks of the slab after earthquake are shown in Fig. 10(b). Note that the slab is partitioned into strips by vertical joints. Thus, as the slab bends in the axial direction,

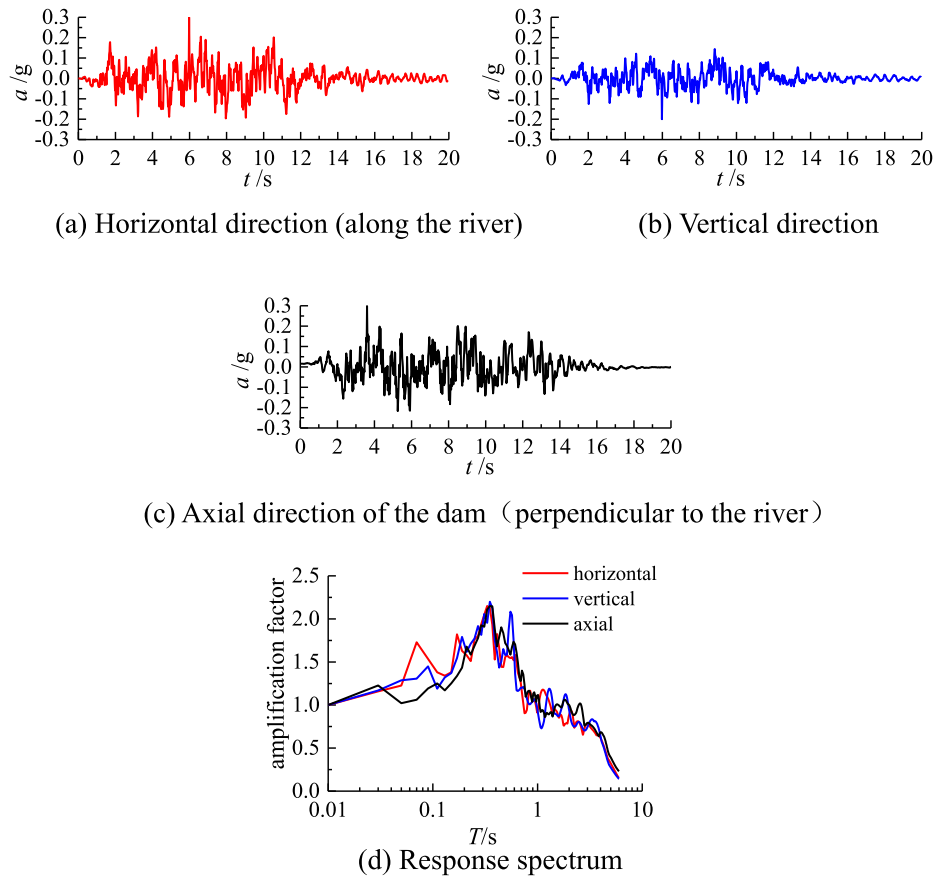


Fig. 5. Acceleration history and response spectrum of input ground motion.

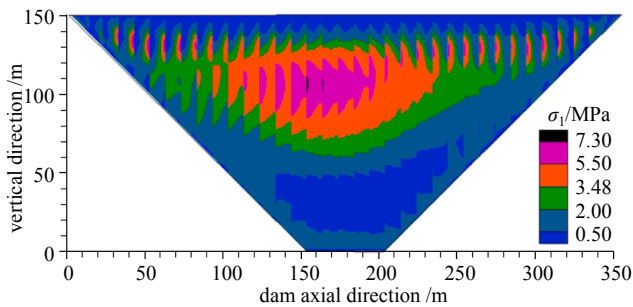


Fig. 6. The envelope of maximum tensile stress during the earthquake (without CIEs, including static stresses).

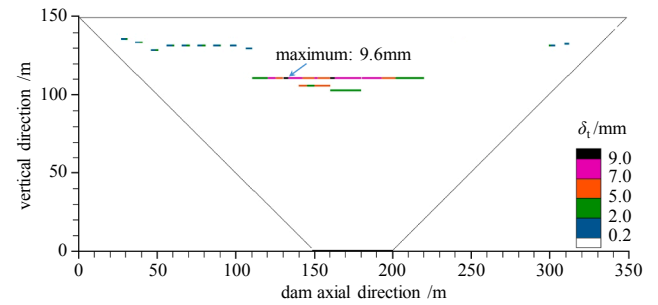


Fig. 8. Distribution of maximum crack during earthquake (with CIEs).

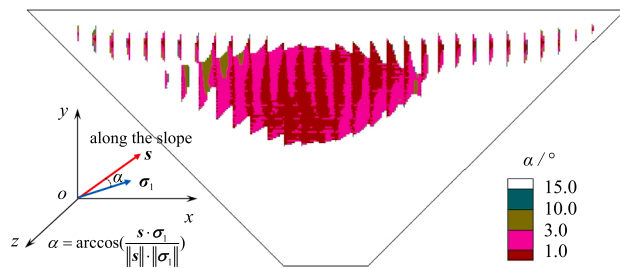


Fig. 7. The angle between maximum tensile stress vectors that exceed the tensile strength and the slope of the face slab (without CIEs, including static stresses).

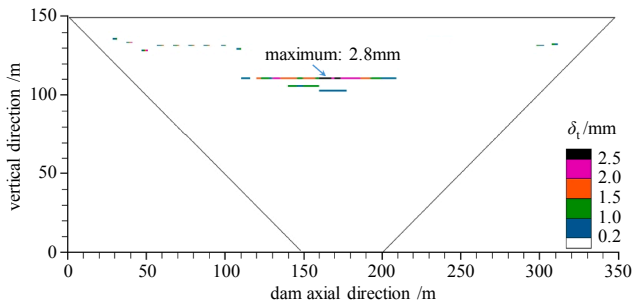
each strip is stretched on the side nearest to the valley and compressed on the side farthest from the valley, as shown in Fig. 10 (a). The deformation causes tensile failure on the side near the valley and leads to the generation of unconnected cracks as shown in Fig. 10 (b).

The residual deformation of dam and the history of displacement along dam axial direction are shown in Fig. 11. The figure shows the presence of plastic deformation in the rockfill on both sides. The deformation is directed towards the valley along the dam axial direction during the earthquake. The histories of the stress and crack width of the CIE at point A are shown in Fig. 12. The stresses during the earthquake are composed of three parts: 1) static stress σ_0 before earthquake; 2) recoverable cyclic stress σ_e caused by seismic load; 3) unrecoverable stress σ_p caused by plastic deformation of the rockfill. The slab is compressed before earthquake ($\sigma_0 < 0$) while σ_p gradually increases due to the plastic deformation of rockfill in dam axial direction (Fig. 11). The recoverable stress σ_e can reduce the safety of the structure at certain moments of the earthquake. The tensile stress is released upon the

Table 6

The maximum crack during earthquake.

Item	Left	Middle			Right
Elevation (H is dam height)	$0.85H$	$0.7H$	$0.72H$	$0.75H$	$0.85H$
Range (in dam axial direction)	30–110	160–180	140–160	110–220	300–312
property	unconnected	connected	connected	connected	unconnected
cumulative length/m	39	20	20	110	6
maximum width/mm	<5	<5	<7	9.6	<3

**Fig. 9.** Residual crack distribution in face slab after the earthquake (with CIEs).**Table 7**

The residual crack after earthquake.

Item	Left	Middle			Right
Elevation (H is dam height)	$0.85H$	$0.7H$	$0.72H$	$0.75H$	$0.85H$
Cumulative length/m	30	20	20	95	4
Maximum width/mm	<3	<1.5	<1.5	2.8	<3

cracking of the slab, as shown in Fig. 12. Because the slab failure is mainly caused by plastic deformation, the crack width does not vary much.

4.2.2. Middle of the slab: connected cracks

The deformation and cracking of the middle face slab at several representative moments are shown in Fig. 13. The face slab is stretched along the slope direction, resulting in the formation of similar tensile stresses in the cross section. Therefore, the cracks are connected across each strip of slab as shown in Fig. 13(b) and (c).

The displacement history of the rockfill along slope direction is shown in Fig. 14. Most of the displacement activity is contributed by the recoverable cyclic deformation caused by the seismic load. The stress

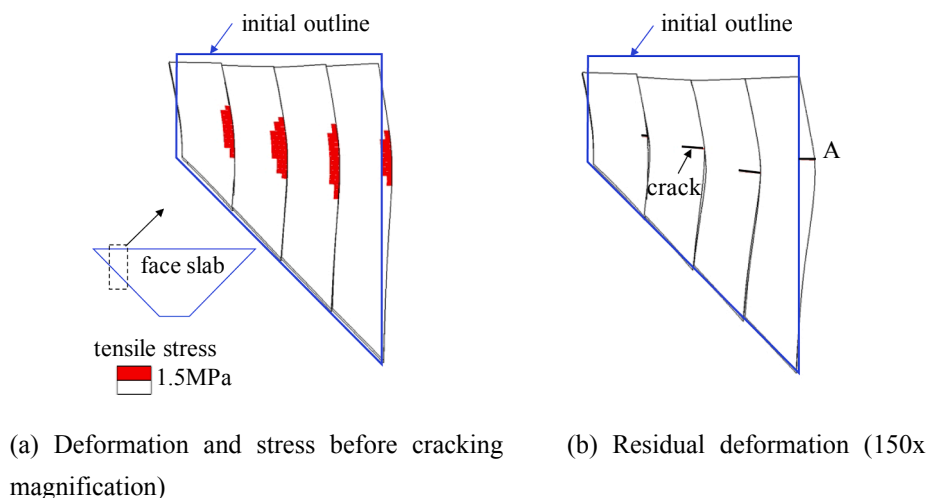
and crack width of the CIE at point B are shown in Fig. 15. Consistent with the displacement of rockfill, σ_e constitutes a major part of the stress during the earthquake. Therefore, the crack opens and closes frequently.

4.2.3. Challenges of the equivalent linear analysis

The region of vulnerability for the slab under seismic activity as estimated through traditional equivalent linear analysis is shown in Fig. 16. The failure of the slab in the valley can be primarily attributed to the recoverable cyclic stress caused by the earthquake. Therefore, compared with the result (Fig. 8) from the elasto-plastic method, the predicted vulnerable locations in the valley are similar, but the areas are smaller due to the inability to describe plastic deformation. More importantly, plastic deformation is the major cause of failure on both sides of face slab. In contrast, the equivalent linear analysis predicted that both sides are safe. In conclusion, traditional equivalent linear analysis can overestimate the seismic safety of the slab due to the inability to describe plastic deformation.

4.3. Interaction between reinforcement and concrete

The histories of the concrete stress, the stiffness degradation factor, the cracking width and the steel stress at the maximum cracking width in the face slab is shown in Fig. 17. Before the damage ($t = 3.86$ s), the results obtained by the CZM and the elastic model are consistent. The unidirectional reinforcement ratio of the reinforcement is 0.6%, and the rigidity on the slab section is $200 \times 0.6\% = 1.2$ GPa, which is about 4% of the concrete elastic modulus (31 GPa). Before the concrete becomes damaged, the tensile force of the reinforcement is only 22 MPa, which is equivalent to the section stress of $22 \times 0.6\% = 0.13$ MPa. Therefore, the reinforcement cannot prevent the occurrence of concrete damage. At 3.86 s, the CIE is damaged with the degradation of rigidity and the strain softening of the concrete. At this time, the tensile stress of the steel experiences a sharp increase. The tensile stress of the concrete computed through elastic model is 3.95 MPa, which is greater than the tensile strength of concrete. As the seismic activity becomes more intense, the damage done to the concrete becomes more severe. At 4.94 s, the

**Fig. 10.** Deformation and stress of the left part of the slab during the earthquake.

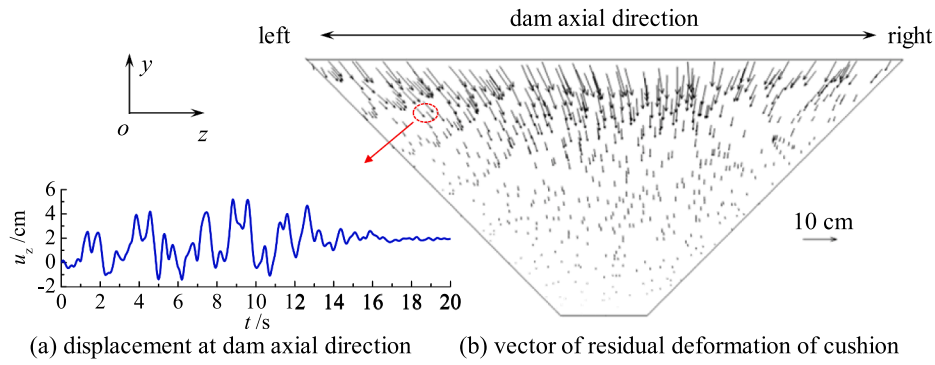
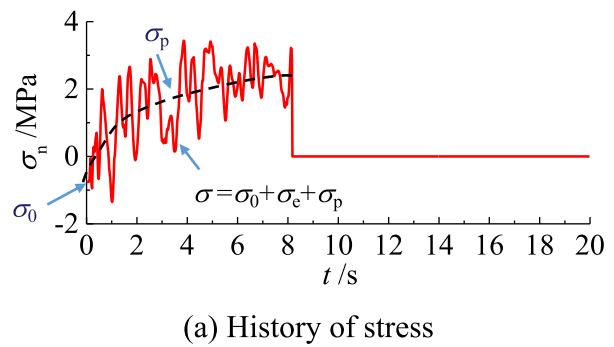
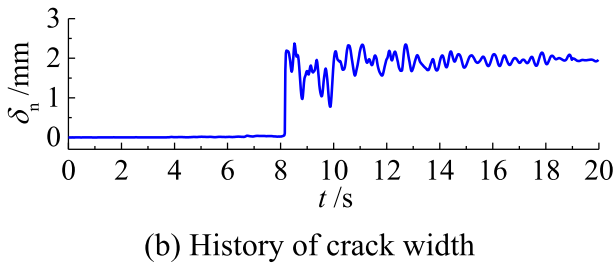


Fig. 11. Deformation of rockfill during the earthquake.



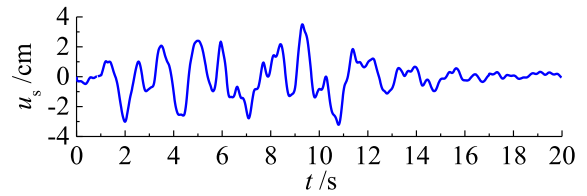
(a) History of stress



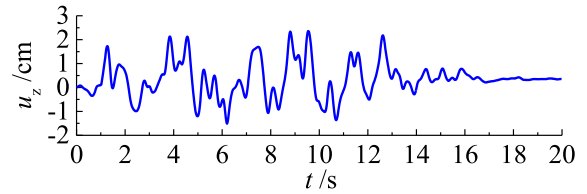
(b) History of crack width

Fig. 12. History of stress and crack width at point A.

concrete is completely fractured, whereupon the tensile rigidity and strength are completely lost. The steel has yielded, but can still bear the tensile stress, which limits the development of cracks. Therefore, the CZM can be used to evaluate the effect of anti-seismic measures. The maximum tensile stress of the concrete computed using the elastic model



(a) Displacement along the slope of face slab



(b) Displacement along the dam axial direction

Fig. 14. History of cushion deformation behind middle slab.

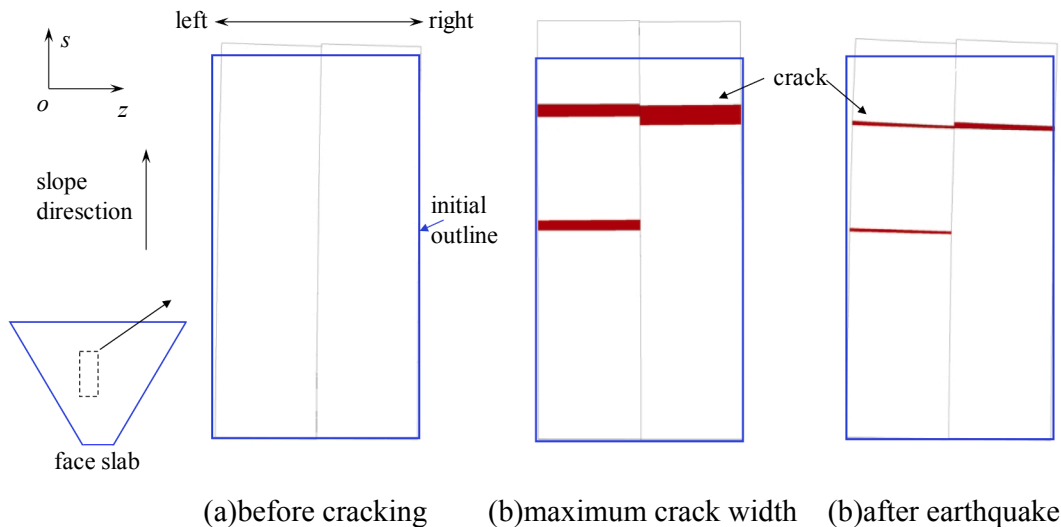


Fig. 13. Deformation of the middle slab (200x magnification).

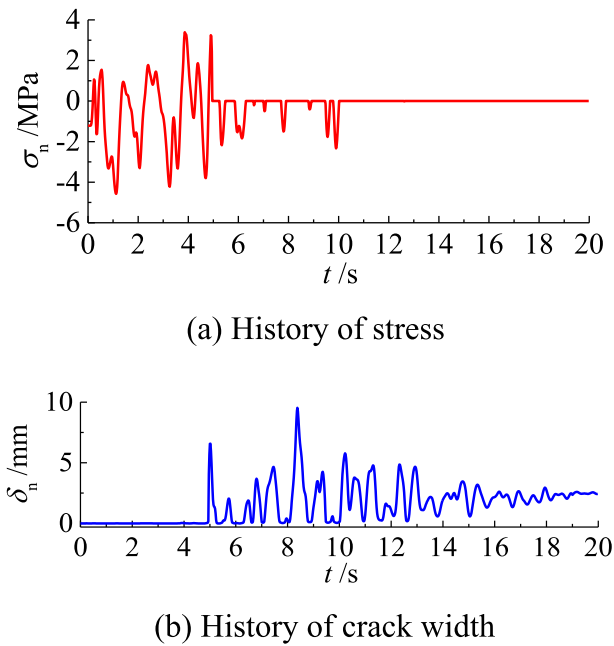


Fig. 15. History of stress and crack width during the failure of an element at the middle slab.

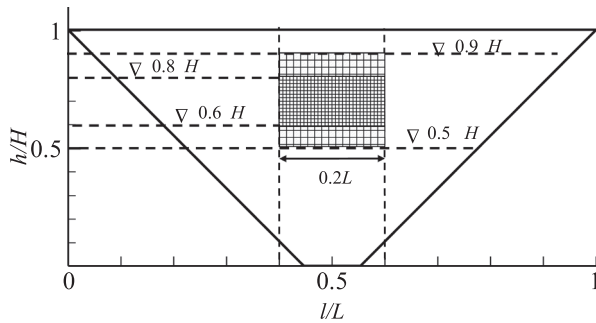


Fig. 16. Extent of the tensile overstressed area due to seismic activity as estimated by equivalent linear analysis.

reaches 6.6 MPa and exceeds the tensile strength of concrete at multiple time instances. The maximum tensile stress of the reinforcement is only 44 MPa, and its strength and toughness cannot be fully used. Therefore, it is impossible to evaluate the effect of seismic reinforcement when the elastic model is used for concrete.

5. Anti-seismic measures

Seismic damage to concrete face slab can be attributed to two issues: one issue is the poor tensile strength and toughness of concrete, and the other issue is the high seismic tensile stresses caused by both the tensile deformation along the slope direction and the bending deformation in the dam axial direction. Therefore, the seismic damage of the concrete slab can be alleviated through two approaches: material property improvement (i.e. increasing reinforcement ratio) and structural optimization (i.e. optimizing width of slab and setting horizontal joint).

5.1. Increasing reinforcement ratio to improve bearing capacity

The traditional elastic analysis for face slab cannot fully describe the failure characteristics of concrete and evaluate the effect of reinforcement. In contrast, the method established in this paper can adequately model the concrete-reinforcement interaction and is thus used to study

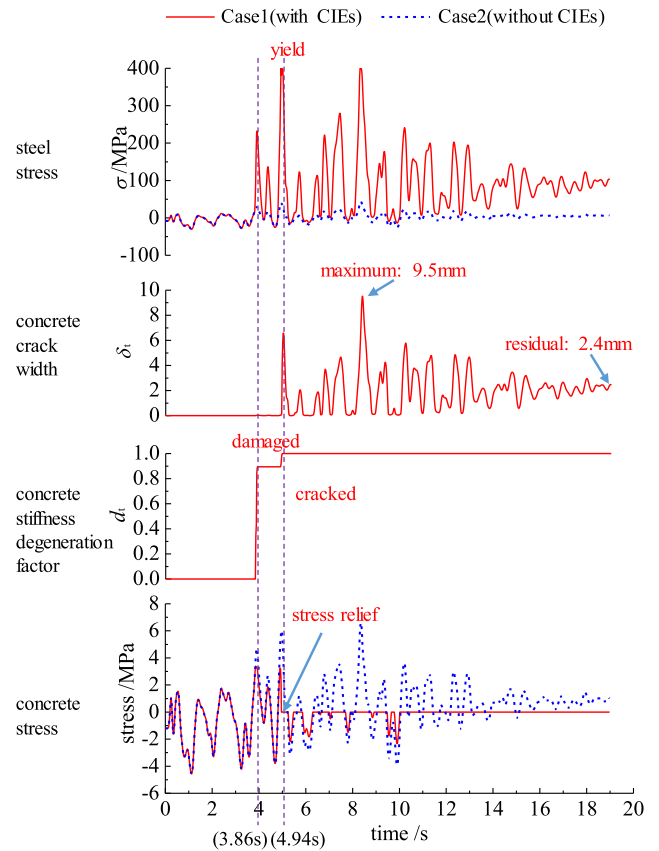


Fig. 17. History of tensile stress, stiffness degradation factor and crack width of concrete, along with the steel stress.

the effect of reinforcement ratio.

The bidirectional reinforcement ratio in the concrete face slab increased from 1.2% to 1.6%. The distribution of residual cracks after earthquake is shown in Fig. 18 which is. There are two connected horizontal cracks near $0.7H$ in the middle of the face slab with a total length of 70 m and a maximum width of 1.6 mm. There are unconnected horizontal cracks at $0.85H$ on left side of the slab with a total length of 8 m. With the increase of the reinforcement ratio, the cracking mode of the face slab remains unchanged; however, the crack length and the maximum crack width respectively decreases by 53.8% and 42.8%. The 2D dynamic analysis by Arici (2013) also showed that increasing the reinforcement ratio is the most effective countermeasure to limit the damage on the face plate.

5.2. Decreasing the width of slab to improve stress state

The analyses in Section 4.2(1) suggests that the tensile stresses on

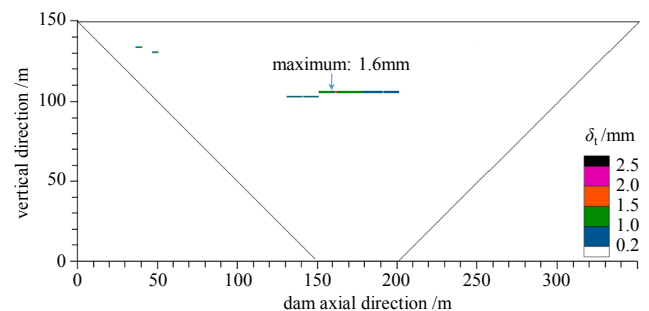


Fig. 18. Distribution of residual crack after earthquake with the reinforcement ratio increasing from 1.2% to 1.6%.

both sides of slab is caused by the bending in the dam axial direction. Therefore, it is feasible to reduce the width of the slab at both sides (i.e. reduce the “height” of the slab in the bending direction) to improve the stresses of the face slab. As shown in Fig. 19, the width of slab on both sides is reduced from 10 m to 5 m while the width in the valley is unchanged. The simulated residual cracks are shown in the Fig. 20. There are unconnected horizontal cracks at $0.85H$ on left side of the slab and have a total length of 12 m. There is no damage in the right side. Otherwise, the crack distribution of the face slab in the valley remains almost unchanged.

Comparing Fig. 9 with Fig. 20, both the crack lengths and widths are reduced after the width of slab are optimized. Fig. 21 (a) and (b) show the stresses and crack widths of representative elements. The reduction of the width decreases the bending stress. Therefore, the crack width of observation element C is decreased by 48.1% (from 2.7 mm to 1.4 mm) as shown in Fig. 21 (a). In addition, the tensile stresses in certain zones are lower than the tensile strength, such as in observation element D as shown in Fig. 21 (b). The reduction in stress reduces the chance of failure in the face slab during earthquake. The crack lengths at both sides of face slab decrease by 64.7%. Research from Sarmiento-Solano and Romo (2019) indicated that decreasing the width of the face slab is also conducive to improving dynamic compressive stress of the face slab. Therefore, reducing the width of face slab on both sides therefore improved the seismic safety of the face slab.

5.3. Horizontal joint to release tensile stress

From the analysis in Section 4.2.2, the middle slab is damaged by tensile deformation along the slope. Therefore, an alternative solution to improve the seismic safety of the face slab is stress relief. Zhang et al. (2017) proposed installing a horizontal joint from 0.35 to $0.65L$ (L is the axial length of dam) at the range $0.7-0.9H$ to release the tensile stress on the face slab. In this section, a horizontal joint is used as an anti-seismic measure for the slab located at middle of the valley, and the effect of the joint is quantitatively evaluated. The horizontal joint is set at a dam height of $0.8H$ and from 0.35 to $0.65L$ of the dam axial direction, as shown in Fig. 22. The material parameters of the horizontal joint are identical to the material parameters of the vertical joints.

The distribution of residual cracks after the earthquake is shown in Fig. 23. The horizontal connected cracks occur at both ends of the horizontal joint. The length of the left crack is 10 m, and the maximum width of the crack is 1.1 mm. The length of the right crack is 12 m with a maximum width of 2.4 mm. The failure mode of the slab on both sides remains almost unchanged. After including the anti-seismic measure, the crack length and maximum width of the slab at the valley are reduced by 83.7% and 14.3% respectively, which represents a significant reduction in the degree of seismic damage. Zhang et al. (2017) investigated the effect of horizontal joints on a face slab through performing equivalent linear analysis and using an elastic model of concrete. The results indicated that the maximum dynamic tensile stresses in the slab decreased 36.8% (from 14.7 MPa to 9.4 MPa) with the inclusion of the horizontal joint. This paper also reports a similar finding.

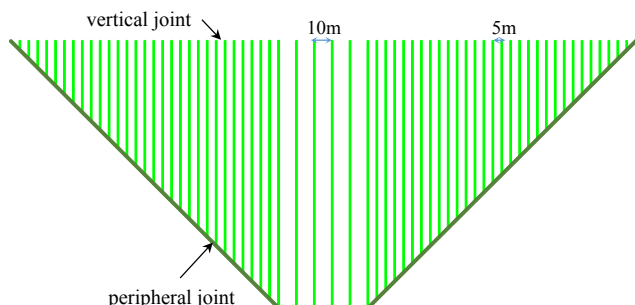


Fig. 19. Vertical joints after optimization.

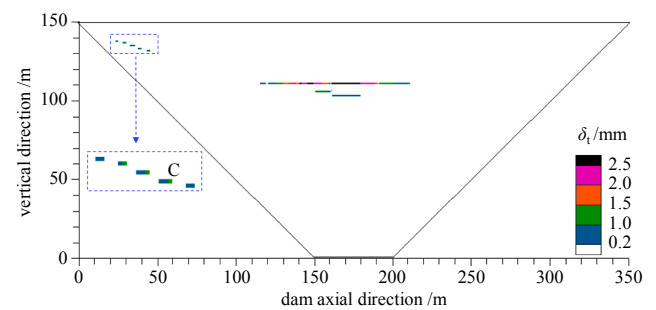


Fig. 20. Distribution of residual cracks with the width of slab decreasing from 10 m to 5 m.

The excessive tensile stress (9.4 MPa) in the concrete face slab is impractical, and the elastic analysis from literature is only a qualitative assessment. On the other hand, the efforts reported in this paper quantifies the effect of anti-seismic measures.

5.4. Comprehensive anti-seismic measures

Increasing the ratio of reinforcement, reducing the width of face slab on both sides and installing a horizontal joint can mitigate the seismic damage experienced by the face slab. In this section, the above three schemes are integrated as comprehensive anti-seismic measures for the concrete face slab. The distribution of residual crack for the modified slab is shown in Fig. 24. Horizontal, unconnected cracks form on the left side of the slab. The cracks have a total of 7 m in length and have a maximum crack width of 0.8 mm. A horizontal, connected crack forms on the right side of the horizontal joint, and possesses a length of 10 m and a maximum width of 2.2 mm. After adopting the comprehensive anti-seismic measures, the maximum crack width decreases by 21% from 2.8 mm to 2.2 mm, and the total crack length decreases by 89.9% from 169 m to 17 m, which greatly improves the seismic safety of face slab.

6. Conclusion

In this paper, the concrete cohesive zone model and explicit method are expanded to perform the 3D seismic failure analysis of a CFRD. Furthermore, a method to investigate the 3D elasto-plastic seismic cracking evolution of a CFRD concrete face slab is proposed by integrating a generalized plastic model of rockfill, a state-dependent elasto-plastic model of soil-structure interface, FEM-SBFEM coupled cross-scale analysis method and a non-uniform wave input method. A 150 m high 3D CFRD is analyzed by the proposed method to perform a refined and computationally efficient investigation of the seismic failure mechanism and failure characteristics of the concrete face slab. The different types of anti-seismic measures are proposed and adopted to mitigate the seismic damage, and their effects are evaluated quantitatively. The following conclusions can be drawn based on the results:

- (1) The middle of the slab is damaged in the form of horizontal, connected cracks at $0.7-0.75H$ (H is the dam height). Meanwhile, horizontal, unconnected cracks occur at $0.85H$ on both sides of face slab. The middle slab is thus the most vulnerable area during an earthquake as demonstrated by the larger crack dimensions and lower elevation than the cracks located at either side.
- (2) The slab on both sides of the dam bends in the dam axial direction due primarily to the plastic deformation of rockfill towards to valley; therefore, each strip of the slab (i.e. slab partitions separated by vertical joints) is stretched on the side near the valley and compressed on the side away from the valley. The opposing deformation results in unconnected cracks. The middle slab is stretched along the slope direction due to cyclic, recoverable

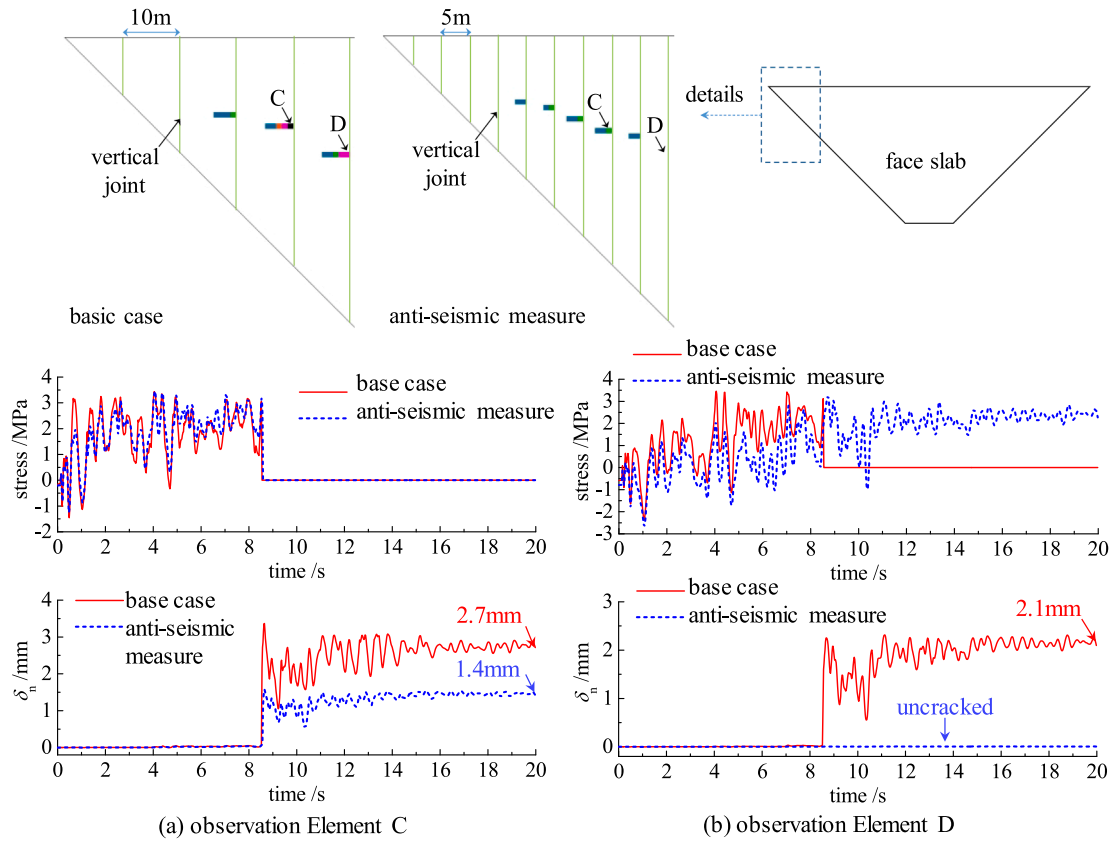


Fig. 21. Comparison of stress and crack width with different width of slab.

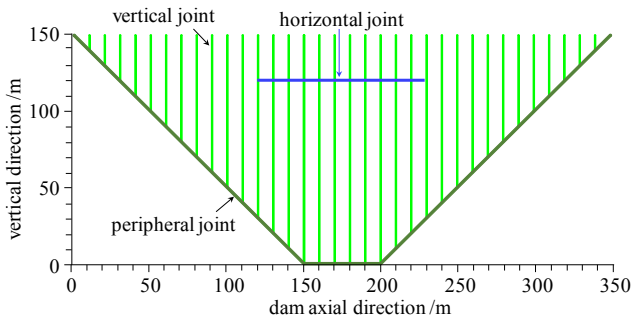


Fig. 22. Position of horizontal joint.

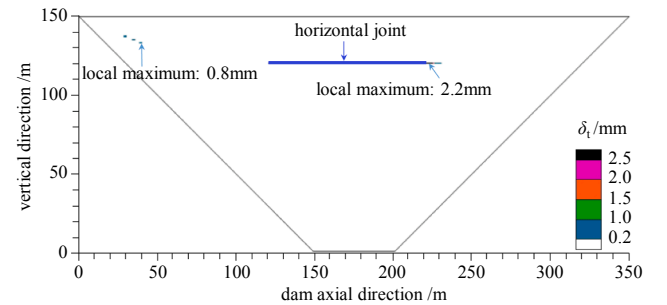


Fig. 24. Distribution of residual crack with comprehensive anti-seismic measure.

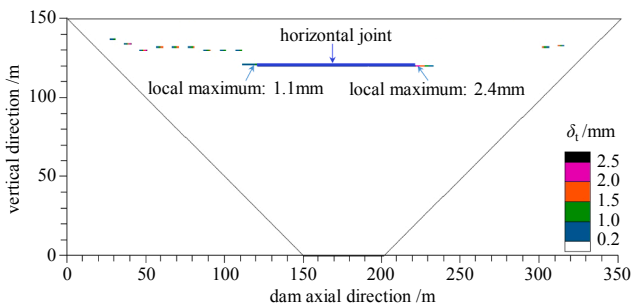


Fig. 23. Distribution of residual crack with a horizontal joint installed.

deformation of the rockfill as caused by seismic loads. The stretching leads to the development of similar tensile stresses in the slab cross section and the formation of connected cracks in

each strip of the slab. Traditional equivalent linear analysis cannot describe the evolution of plastic deformation and will therefore overestimate the seismic safety of the slab.

- (3) When the reinforcement ratio of concrete face slab is increased from 1.2% to 1.6%, the crack length and maximum crack width are decreased by 53.8% and 42.8%, respectively. The tensile stresses caused by the bending deformation is reduced by decreasing the width of face slab on both sides (i.e. from 10 m to 5 m), and the length and maximum width of cracks are reduced by 64.7% and 48.1%, respectively. A horizontal joint installed in the upper-middle part of the slab can effectively release earthquake-induced tensile stresses. With the horizontal joint, the length and maximum width of the cracks can be reduced by 14.3% and 83.7%, respectively. By combining the above three anti-seismic measures, the maximum crack width of slab decreases by 21% from 2.8 mm to 2.2 mm, and the total crack

length decreases by 89.9% from 169 m to 17 m, which greatly improves the seismic safety of the face slab.

- (4) The proposed method can describe the evolution of cracks in the slab during earthquakes, accurately locate seismically vulnerable areas of the slab, evaluate the effect of anti-seismic measures, and provide an intuitive and quantitative slab seismic assessment. The method overcomes the limitations of strength-based traditional linear elastic analyses. The method provides an effective way for further analysis of the ultimate seismic capacity for CFRDs, and can be applied to the seismic failure analyses of other concrete structures (e.g. cut-off walls, pile foundations, tunnels) that experience soil-structure interaction.

CRedit authorship contribution statement

Yongqian Qu: Software, Methodology, Formal analysis, Investigation, Data curation, Writing – original draft, Visualization. **Degao Zou:** Conceptualization, Software, Methodology, Validation, Writing - review & editing, Project administration, Funding acquisition. **Kai Chen:** Methodology, Writing - review & editing. **Jingmao Liu:** Validation, Resources.

Declaration of Competing Interest

The authors declare that they have no known competing financial interests or personal relationships that could have appeared to influence the work reported in this paper.

Acknowledgements

The research work described in this paper was supported by the National Natural Science Foundation of China (Grant Nos. U1965206 and 52079023) and the China Postdoctoral Science Foundation (Grant Nos. BX20200074 and 2021M690520). The writers would like to greatly acknowledge all the financial support and express their sincerest gratitude.

References

- Ahmadi, S.F., Eskandari, M., 2013. Comments on "Mathematical analysis for an axisymmetric disc-shaped crack in transversely isotropic half-space, International Journal of Mechanical Sciences 68 (2013) 171–179, by Morteza Eskandari-Ghadi, Azizollah Ardeshir-Behrestaghi, Bahram Navayi Neyra". *Int. J. Mech. Sci.* 75, 156–157.
- Ahmadi, S.F., Eskandari, M., 2014. Vibration analysis of a rigid circular disk embedded in a transversely isotropic solid. *J. Eng. Mech.* 140 (7), 04014048. [https://doi.org/10.1061/\(ASCE\)JEM.1943-7889.0000757](https://doi.org/10.1061/(ASCE)JEM.1943-7889.0000757).
- Ahmadi, S.F., Samea, P., Eskandari, M., 2016. Axisymmetric response of a bi-material full-space reinforced by an interfacial thin film. *Int. J. Solids Struct.* 90, 251–260.
- Alfano, G., 2006. On the influence of the shape of the interface law on the application of cohesive-zone models. *Compos. Sci. Technol.* 66 (6), 723–730.
- Arici, Y., 2011. Investigation of the cracking of CFRD face plates. *Comput. Geotech.* 38 (7), 905–916.
- Arici, Y., 2013. Evaluation of the performance of the face slab of a CFRD during earthquake excitation. *Soil Dyn. Earthquake Eng.* 55, 71–82.
- Barenblatt, G.I., 1962. The mathematical theory of equilibrium cracks in brittle fracture. *Adv. Appl. Mech.* 7, 55–129.
- Boulanger, R.W., Bray, J.D., Merry, S.M., Mejia, L.H., 1995. Three-dimensional dynamic response analyses of Cogswell Dam. *Can. Geotech. J.* 32 (3), 452–464.
- Cen, W.-J., Wen, L.-S., Zhang, Z.-q., Xiong, K., 2016. Numerical simulation of seismic damage and cracking of concrete slabs of high concrete face rockfill dams. *Water Sci. Eng.* 9 (3), 205–211.
- Chen, K., Zou, D., Kong, X., Chan, A., Hu, Z., 2017. A novel nonlinear solution for the polygon scaled boundary finite element method and its application to geotechnical structures. *Comput. Geotech.* 82, 201–210.
- Chen, K., Zou, D., Kong, X., Zhou, Y., 2018a. Global concurrent cross-scale nonlinear analysis approach of complex CFRD systems considering dynamic impervious panel-rockfill material-foundation interactions. *Soil Dyn. Earthquake Eng.* 114, 51–68.
- Chen, K., Zou, D., Kong, X., Yu, X., 2018b. An efficient nonlinear octree SBFEM and its application to complicated geotechnical structures. *Comput. Geotech.* 96, 226–245.
- Chen, K., Zou, D., Kong, X., Liu, J., 2019. Elasto-plastic fine-scale damage failure analysis of metro structures based on coupled SBFEM-FEM. *Comput. Geotech.* 108, 280–294.
- Chen, K., Zou, D., Tang, H., Liu, J., Zhuo, Y., 2021. Scaled boundary polygon formula for Cosserat continuum and its verification. *Eng. Anal. Boundary Elem.* 126, 136–150.
- Dai, Q., Ng, K., 2014. 2D cohesive zone modeling of crack development in cementitious digital samples with microstructure characterization. *Constr. Build. Mater.* 54, 584–595.
- Dakoulas, P., 2012. Longitudinal vibrations of tall concrete faced rockfill dams in narrow canyons. *Soil Dyn. Earthquake Eng.* 41, 44–58.
- Dugdale, D.S., 1960. Yielding of steel sheets containing slits. *J. Mech. Phys. Solids* 8 (2), 100–104.
- Evgin, E., Fakharian, K., 1996. Effect of stress paths on the behaviour of sand steel interfaces. *Can. Geotech. J.* 33 (6), 853–865.
- Feng, D., Zhang, G., Zhang, J., 2010. Three-dimensional seismic response analysis of a concrete-faced rockfill dam on overburden layers. *Front. Arch. Civil Eng. China* 4 (2), 258–266.
- Gong, J., Zou, D., Kong, X., Qu, Y., Liu, J., 2019. An extended meshless method for 3D interface simulating soil-structure interaction with flexibly distributed nodes. *Soil Dyn. Earthquake Eng.* 125, 105688. <https://doi.org/10.1016/j.soildyn.2019.05.027>.
- Hillerborg, A., Modér, M., Petersson, P.-E., 1976. Analysis of crack formation and crack growth in concrete by means of fracture mechanics and finite elements. *Cem. Concr. Res.* 6 (6), 773–781.
- Kartal, M.E., Bayraktar, A., Ba?aa, H.B., 2010. Seismic failure probability of concrete slab on CFR dams with welded and friction contacts by response surface method. *Soil Dyn. Earthquake Eng.* 30(11), 1383–1399.
- Kim, Yong-Seong, Kim, Byung-Tak, 2008. Prediction of relative crest settlement of concrete-faced rockfill dams analyzed using an artificial neural network model. *Comput. Geotech.* 35 (3), 313–322.
- Kim, Yong-Rak, de Freitas, Felipe A.C., Jung, Jong Suk, Sim, Youngjong, 2015. Characterization of bitumen fracture using tensile tests incorporated with viscoelastic cohesive zone model. *Constr. Build. Mater.* 88, 1–9.
- Kong, Xianjing, Zhou, Yang, Zou, Degao, Xu, Bin, Yu, Long, 2011. Numerical analysis of dislocations of the face slabs of the Zipingpu concrete faced rockfill dam during the Wenchuan earthquake. *Earthquake Eng. Eng. Vib.* 10 (4), 581–589.
- Kong, X., Zou, D., Liu, J., 2016. Developments in seismic safety evaluation methods and aseismic measures for high rockfill dams. *J. f Hydroelectric Eng.* 35 (7), 1–14.
- Li, Xiaobao, Jiang, Lijian, Mi, Changwen, 2020. Flamant solution of a half-plane with surface flexural resistibility and its applications to nanocontact mechanics. *Math. Mech. Solids* 25 (3), 664–681.
- Liu, Jun, Lin, Gao, 2012. A scaled boundary finite element method applied to electrostatic problems. *Eng. Anal. Boundary Elem.* 36 (12), 1721–1732.
- Liu, J., Kong, X., Zou, D., 2015. Effects of interface models on deformation of interface between slab and cushion layer and slab stress of concrete faced rock fill dam. *Chinese J. Geotech. Eng.* 37 (4), 700–710.
- Liu, Jun, Zhang, Pengchong, Lin, Gao, Wang, Wenyuan, Lu, Shan, 2016. Solutions for the magneto-electro-elastic plate using the scaled boundary finite element method. *Eng. Anal. Boundary Elem.* 68, 103–114.
- Liu, Jingmao, Zou, Degao, Kong, Xianjing, 2014. A three-dimensional statedependent model of soil-structure interface for monotonic and cyclic loadings. *Comput. Geotech.* 61, 166–177.
- Liu, J., Du, Y., Du, X., et al., 2006. 3D viscous-spring artificial boundary in time domain. *Earthquake Eng. Eng. Vib.* 5 (1), 93–102.
- Man, H., Song, C., Gao, W., Tin-Loi, F., 2012. A unified 3D-based technique for plate bending analysis using scaled boundary finite element method. *Int. J. Numer. Meth. Eng.* 91 (5), 491–515.
- Pan, Jianwen, Zhang, Chuhan, Xu, Yanjie, Jin, Feng, 2011. A comparative study of the different procedures for seismic cracking analysis of concrete dams. *Soil Dyn. Earthquake Eng.* 31 (11), 1594–1606.
- Pastor, M., Zienkiewicz, O.C., 1986. A generalized plasticity, hierarchical model for sand under monotonic and cyclic loading. In: *Proceedings of the 2nd International Symposium on Numerical Models in Geomechanics*. Ghent, pp. 131–149.
- Pastor, M., Zienkiewicz, O.C., Leung, K.H., 1985. Simple model for transient soil loading in earthquake analysis. II. Non-associative models for sands. *Int. J. Numer. Anal. Meth. Geomech.* 9 (5), 477–498.
- Qu, Yongqian, Zou, Degao, Kong, Xianjing, Xu, Bin, 2017. A novel interface element with asymmetric nodes and its application on concrete-faced rockfill dam. *Comput. Geotech.* 85, 103–116.
- Qu, Yongqian, Zou, DeGao, Kong, XianJing, Xu, Bin, Yu, Xiang, 2018. A flexible various-scale approach for soil-structure interaction and its application in seismic damage analysis of the underground structure of nuclear power plants. *Sci. China Technol. Sci.* 61 (7), 1092–1106.
- Qu, Yongqian, Zou, Degao, Kong, Xianjing, Liu, Jingmao, Zhang, Yu, Yu, Xiang, 2019. Seismic damage performance of the steel fiber reinforced face slab in the concrete-faced rockfill dam. *Soil Dyn. Earthquake Eng.* 119, 320–330.
- Qu, Yongqian, Zou, Degao, Kong, Xianjing, Yu, Xiang, Chen, Kai, 2020. Seismic cracking evolution for anti-seepage face slabs in concrete faced rockfill dams based on cohesive zone model in explicit SBFEM-FEM frame. *Soil Dyn. Earthquake Eng.* 133, 106106. <https://doi.org/10.1016/j.soildyn.2020.106106>.
- Sarmiento-Solano, Nefalí, Romo, Miguel P., 2019. Dynamic in-plane transversal normal stresses in the concrete face of CFRD. *Front. Struct. Civil Eng.* 13 (1), 135–148.
- Shi, Mingguang, Zhong, Hong, Ooi, Ean Tat, Zhang, Chuhan, Song, Chongmin, 2013. Modelling of crack propagation of gravity dams by scaled boundary polygons and cohesive crack model. *Int. J. Fract.* 183 (1), 29–48.
- Trawinski, W., Tejchman, J., Bobiński, J., 2018. A three-dimensional meso-scale modelling of concrete fracture, based on cohesive elements and X-ray μ CT images. *Eng. Fract. Mech.* 189, 27–50.
- Wang, Wei, Zhou, Mozheng, Zhang, Bingyin, Peng, Chong, 2019. A dual mortar contact method for porous media and its application to clay-core rockfill dams. *Int. J. Numer. Anal. Meth. Geomech.* 43 (9), 1744–1769.

- Westergaard, H.M., 1933. Water pressures on dams during earthquakes. *Translator* 98 (2), 418–433.
- Wolf, J.P., Schanz, Martin, 2004. The scaled boundary finite element method. *Comput. Mech.* 33 (4).
- Wolf, J.P., Song, C., 1996. *Finite-Element Modelling of Unbounded Media*. John Wiley.
- Xu, B., Zhou, Y., Zhou, C., et al., 2018. Dynamic responses of concrete-faced rockfill dam due to different seismic motion input methods. *Int. J. Distrib. Sensor Networks* 14 (10), 1550147718804687.
- Xu, Bin, Zou, Degao, Kong, Xianjing, Hu, Zhiqiang, Zhou, Yang, 2015. Dynamic damage evaluation on the slabs of the concrete faced rockfill dam with the plastic-damage model. *Comput. Geotech.* 65, 258–265.
- Xu, Bin, Zou, Degao, Liu, Huabei, 2012. Three-dimensional simulation of the construction process of the Zipingpu concrete face rockfill dam based on a generalized plasticity model. *Comput. Geotech.* 43, 143–154.
- Yang, Suchun, Liu, Junwei, Garg, Ankit, Zhang, Mingyi, 2020. Analytical solution for estimating bearing capacity of a closed soil plug: verification using an on-site static pile test. *J. Marine Sci. Eng.* 8 (7), 490. <https://doi.org/10.3390/jmse8070490>.
- Yilmaz, Okan, Molinari, Jean-François, 2017. A mesoscale fracture model for concrete. *Cem. Concr. Res.* 97, 84–94.
- Zarfl, Christiane, Lumsdon, Alexander E., Berlekamp, Jürgen, Tydecks, Laura, Tockner, Klement, 2015. A global boom in hydropower dam construction. *Aquat. Sci.* 77 (1), 161–170.
- Zhang, J., Hou, W., Zhang, G., et al., 2008. Development and application of 3D soil-structure interface test apparatus. *Chinese J. Geotech. Eng.* 30 (6), 889–894.
- Zhang, Yu, Kong, Xianjing, Zou, Degao, Xu, Bin, 2017. Tensile stress responses of CFRD face slabs during earthquake excitation and mitigation measures. *Int. J. Geomech.* 17 (12), 04017120. [https://doi.org/10.1061/\(ASCE\)GM.1943-5622.0000997](https://doi.org/10.1061/(ASCE)GM.1943-5622.0000997).
- Zhong, Hong, Li, Hongjun, Ooi, Ean Tat, Song, Chongmin, 2018. Hydraulic fracture at the dam-foundation interface using the scaled boundary finite element method coupled with the cohesive crack model. *Eng. Anal. Boundary Elem.* 88, 41–53.
- Zhou, Mozhen, Zhang, Bingyin, Peng, Chong, Wu, Wei, 2016. Three-dimensional numerical analysis of concrete-faced rockfill dam using dual-mortar finite element method with mixed tangential contact constraints. *Int. J. Numer. Anal. Meth. Geomech.* 40 (15), 2100–2122.
- Zhou, Mozhen, Zhang, Bingyin, Peng, Chong, Ronaldo, Borja, 2018. Numerical evaluation of soft inter-slab joint in concrete-faced rockfill dam with dual mortar finite element method. *Int. J. Numer. Anal. Meth. Geomech.* 42 (5), 781–805.
- Zou, Degao, Teng, Xiaowei, Chen, Kai, Liu, Jingmao, 2019. A polyhedral scaled boundary finite element method for three-dimensional dynamic analysis of saturated porous media. *Eng. Anal. Boundary Elem.* 101, 343–359.
- Zou, Degao, Xu, Bin, Kong, Xianjing, Liu, Huabei, Zhou, Yang, 2013. Numerical simulation of the seismic response of the Zipingpu concrete face rockfill dam during the Wenchuan earthquake based on a generalized plasticity model. *Comput. Geotech.* 49, 111–122.
- Zou, D., You, H., Kong, X., et al., 2009. Research on joint simplified model and effects of joint parameters on panel stress and joint displacements of faced rockfill dam. *Chinese J. Rock Mech. Eng.* 28 (S1), 3257–3263.
- Zou, Degao, Zhou, Yang, Ling, Hoe I., Kong, Xianjing, Xu, Bin, 2012. Dislocation of face-slabs of Zipingpu concrete face rockfill dam during Wenchuan earthquake. *J. Earthquake Tsunami* 6 (2), 1250007. <https://doi.org/10.1142/S1793431112500078>.